Abnormal visual gain control in a Parkinson's disease model

Farinaz Afsari[1], Kenneth V. Christensen[3], Garrick Paul Smith[3], Morten Hentzer[3], Olivia M. Nippe[1], Christopher J. H. Elliott[1] and Alex R. Wade[2],*

[1]Department of Biology and [2]Department of Psychology, University of York, YO1 5DD York, UK and [3]Neuroscience Drug Discovery DK, H. Lundbeck A/S, Ottiliavej 9, DK-2500 Valby, Denmark

Our understanding of Parkinson's disease (PD) has been revolutionized by the discovery of disease-causing genetic mutations. The most common of these is the *G2019S* mutation in the *LRRK2* kinase gene, which leads to increased kinase activity. However, the link between increased kinase activity and PD is unclear. Previously, we showed that dopaminergic expression of the human *LRRK2-G2019S* transgene in flies led to an activity-dependent loss of vision in older animals and we hypothesized that this may have been preceded by a failure to regulate neuronal activity correctly in younger animals. To test this hypothesis, we used a sensitive measure of visual function based on frequency-tagged steady-state visually evoked potentials. Spectral analysis allowed us to identify signals from multiple levels of the fly visual system and wild-type visual response curves were qualitatively similar to those from human cortex. Dopaminergic expression of *hLRRK2-G2019S* increased contrast sensitivity throughout the retinal network. To test whether this was due to increased kinase activity, we fed *Drosophila* with kinase inhibitors targeted at LRRK2. Contrast sensitivity in both day 1 and day 14 flies was normalized by a novel LRRK2 kinase inhibitor 'BMPPB-32'. Biochemical and cellular assays suggested that BMPPB-32 would be a more specific kinase inhibitor than LRRK2-IN-1. We confirmed this *in vivo*, finding that *dLRRK⁻* null flies show large off-target effects with LRRK2-IN-1 but not BMPPB-32. Our data link the increased Kinase activity of the G2019S-LRRK2 mutation to neuronal dysfunction and demonstrate the power of the Drosophila visual system in assaying the neurological effects of genetic diseases and therapies.

INTRODUCTION

Although the primary deficits in Parkinson's disease (PD) are related to rigidity, postural instability, bradykinesia and tremor, a wide variety of visual issues have also been reported—ranging from abnormal light adaptation to visual hallucinations (1). The discovery that dopamine plays an active part in signal regulation in the human retina (2,3), and that retinal dopamine is reduced in PD (4), means that some of the visual consequences of PD may originate in the retina—the earliest and most fundamental stage of visual processing.

One problem with assaying visual deficits in human Parkinson's patients is that this is a heterogeneous disease with multiple genetic and environmental origins. A powerful complement to this approach is to dissect the complex neural deficits using the genetically tractable model organism, *Drosophila*. Although flies are

only distantly related to humans in evolutionary terms, many of the neuronal circuits in the vertebrate and fly eye appear to be analogous. This was first noted by Ramon y Cajal using silver staining (5) and it has been confirmed by more modern cytochemical tools (6). Crucially, both vertebrates and flies have dopaminergic neurons in the visual system (7,8) and dopaminergic circuits modulate fly vision (9,10). It is therefore possible that PD-associated pathogenic mutations may have similar effects on very early visual processing in both flies and humans.

Here, we focus on a single nucleotide polymorphism in the *LRRK2* gene (*G2019S*). This is carried by a relatively large proportion of human PD patients, 3–40%, depending on ethnicity (11), making it the most common genetic cause of PD. Nonetheless, the role of the LRRK2 protein in the pathogenesis of PD is unclear (12). Manipulations of *LRRK2* in mouse have not generated robust neuronal phenotypes (13), with the most marked

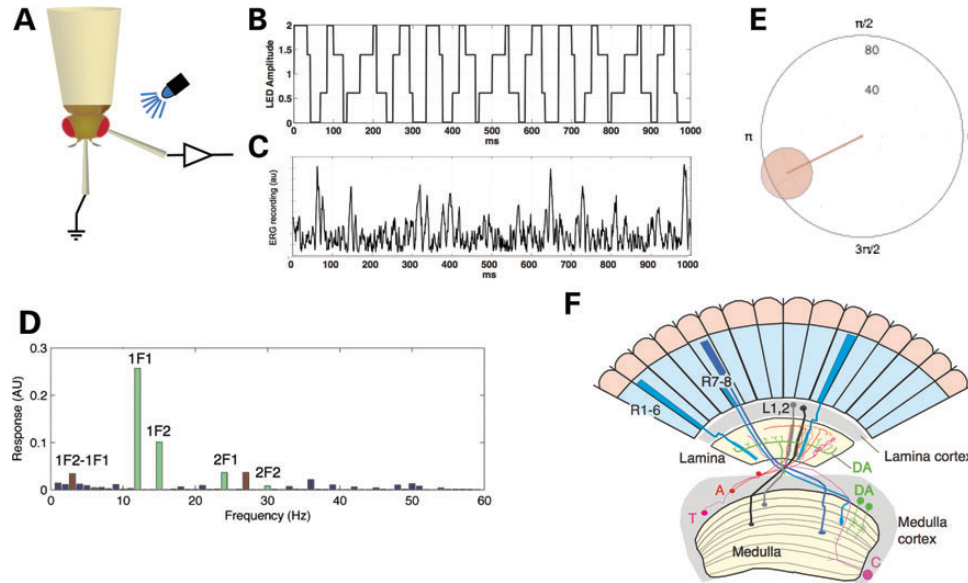*To whom correspondence should be addressed. Email: wade@wadelab.net

Figure 1. Recording and analysing the visual response with SSVEP. (**A**) Flies are restrained in a Gilson pipette tip and illuminated by a blue, light-emitting diode (LED) is driven with by a continuously flickering wave. Electrodes on the eye and mouth record the response of the visual network. The signal is amplified and digitized. (**B**) The stimulus is the sum of 2 square waves (1F1 and 1F2). (**C**) A typical recording, showing 1 s of data from a single trial in one white-eyed fly. (**D**) The response is separated out into its separate parts by frequency. In this experiment, the stimulus had two input frequencies (12 and 15 Hz). Harmonics of the inputs are shown in the Fourier transform of the signal as green bars. Low-order intermodulation terms (e.g. 1F2-1F1, 2F1+2F2) are shown in brown. (**E**) Responses at any given frequency have a complex phase as well as an amplitude. This can be illustrated in a polar plot where amplitude is mapped along the radial direction and *decreasing* angle in the clockwise direction indicates *increasing* phase lag. Here, the response to a 60% contrast measured at 1F1 in a mutant phenotype is illustrated. The shaded circle indicates the complex standard error of the mean computed across individual flies. (**F**) Diagram of the structure of the fly visual system. This includes the photoreceptors and the second-order amacrine (A) and lamina neurons (L1, L2). It also shows two types of medulla neurons (C and T) that project to the lamina. The visual lobes also include dopaminergic cells (DA), some intrinsic to the medulla, others projecting from the CNS to the lamina. For each category of neuron, only one or two representative cells are shown. Diagram based on silver staining (23) and dopaminergic reporters (9).

responses suggesting abnormal kidney function (14). However, expressing a range of LRRK2 transgenes in the fly has revealed mitochondrial and synaptic phenotypes (15–17). Recently, our group (9) showed a highly selective response to *LRRK2-G2019S* expression in fly dopaminergic neurons: a loss of visual response and degeneration of the retina in old flies. This was not seen with the expression of wild-type *hLRRK2* or other *hLRRK2* mutations.

What leads to this loss of visual function? We showed that the degeneration was accelerated by increased neuronal activity (9) and hypothesized that young G2019S flies could be shown to have amplified neuronal response, if only a more sensitive assay were available. In human visual electrophysiology, the steady-state visual evoked potential (SSVEP) method is a sensitive technique that is often used to measure neuronal response amplitudes in both adults and more challenging populations such as infants. In the SSVEP assay, responses to flickering patterns are routinely recorded by an array of electrodes and their signals used to compute the visual sensitivity. Sensitivity is high because responses to many hundreds of stimulus events are averaged together and out-of-band noise is eliminated from the analysis. In this article, we develop an SSVEP assay for *Drosophila* retina and show it is sensitive enough to demonstrate that one-day-old flies expressing *LRRK2-G2019S* in their dopaminergic neurons already have abnormal visual neurotransmission. A similar approach has been used to examine the processing of visual signals in the fly brain (18–20).

The discovery (in biochemical assays) that the *G2019S* mutation increases the kinase activity of LRRK2 (21) has led to the development of several potential kinase inhibitors that may

provide the basis for novel therapeutic approaches. These could potentially be of great value, as the current symptomatic PD treatment by L-DOPA is time-limited and does not delay disease progression. We therefore used our novel SSVEP assay to do a 'first in vivo' test of two kinase inhibitors targeted at LRRK2. One inhibitor 'BMPPB-32' is a new LRRK2 reference compound characterized by high specificity and selectivity to the LRRK2 kinase domain (see Supplementary Material, Material and Methods). The other compound, 'LRRK2-IN-1', is a leading LRRK2 kinase inhibition reagent in biochemical assays, first described in ref. (22). We find that both compounds ameliorate the abnormal visual phenotypes associated with the G2019S mutation.

Finally, the ideal therapeutic compound should be specific for the kinase domain of LRRK2, and not affect other kinases. Achieving this selectivity is possible but challenging because of the more or less conserved nature of the ATP-binding pocket in vertebrate kinases. To test our compounds for non-specific kinase effects, we applied them to the $dLRRK^-$ null fly and used the sensitive SSVEP assay to show that LRRK2-IN-1 has stronger off-target effects than BMPPB-32. Our SSVEP approach therefore highlights the possibilities of the *Drosophila* visual system as an effective model for genetic and therapeutic analysis of visual responses related to human vision.

RESULTS

Contrast-driven SSVEP responses in Drosophila

We recorded the response of the fly visual system to a preprogrammed sequence of frequency-tagged flickering stimuli

(Fig. 1). This type of stimulus is commonly used in electrophysiological experiments because it generates frequency- and phase-locked response components with a very high signal-to-noise ratio (19,20,24–28). Our first goal is to understand how the response relates to neural activity in each of the components of the visual pathway (Fig. 1F). In *Drosophila*, the response is mediated by the retinal photoreceptors which synapse onto the second-order neurons. Some second-order neurons, the amacrine cells, mediate lateral interactions in the network, but the main lamina neurons project to the third-order cells in the medulla. Since the retinal, lamina and medulla neurons are effectively electrically linked in series (29), all of these neurons may contribute to the waveform. The responses from these different stages can, in theory, be disambiguated by the different components they generate in the frequency domain, and this can be confirmed by genetic dissection of the retinal network.

In SSVEP experiments, each frequency-tagged stimulus component with a fundamental frequency of F generates a set of peaks at multiples of F. For example, in Figure 1D, the responses to the input components at 12 and 15 Hz are evident at 12, 15, 24 and 30 Hz. These are coded in green. In this article, we adopt the nomenclature used in previous papers (27,30) when referring to frequency components: each component is identified by the code [harmonic]F[input] where [input] indexes the different input categories (1 = probe, 2 = mask) and [harmonic] indicates the multiple of each input fundamental. For example, the component corresponding to the second harmonic of the 'probe' component is 2F1, while the third harmonic of the 'mask' component would be 3F2.

The largest responses to the inputs are typically found at the first and second harmonics: '1F' and '2F'. For the first input frequency component that we call the 'probe', these frequencies correspond to 12 and 24 Hz ('1F1' and '2F1').

Signals that respect the polarity of the input can be thought of as weighted Fourier components of the square wave that we use to drive the photoreceptors. These include the first harmonic (1F), and other 'odd multiple' harmonics at 3F, 5F, 7F and so on. They must result from an asymmetric response to the light onset and offset and it is most likely that their primary source is the sustained photoreceptor depolarization event elicited by the onset of the periodic light pulse. 'Even' harmonics (2F, 4F, 6F, . . .) on the other hand must be generated by 'symmetrical' response to either the onset or the offset of light and we therefore propose that their origin lies in the responses of the second-order lamina cells which generate the transient responses that accompany the on- and off-transients of traditional electroretinograms. Finally, responses at low-order sums and differences of the input frequencies must arise from non-linear combinations of the inputs (31,32). These responses (e.g. 2F1+2F2) are most likely to arise from interactions of the lamina and medulla neurons, where non-linear operations such as rectification or divisive normalization at higher levels of visual processing may occur. It is also possible that they derive from a non-linear transducer stage in the retina.

Isolation of photoreceptor and neuronal responses

To test these hypotheses about the physiological origins of the harmonic signature in SSVEP responses, we used genetic knockouts to isolate individual processing stages. The $ort^{-/-}$

knockout mutation inactivates the histamine A receptors on the second-order lamina neurons, thereby preventing photoreceptor → lamina and photoreceptor → amacrine cell signalling (33). The effect of this mutation is very clear in an SSVEP analysis (Fig. 2), where we compare wild-type (*wt*) and $ort^{-/-}$ flies. The 1F1 components in wild-type flies (Fig. 2Ai) are moderately reduced in this *ort* mutant (Fig. 2Aii and iii): at the high end of the contrast range, they are approximately half the wild-type. This reduction in the 1F1 responses may result from the fact that we have abolished the feedback loop from the laminar neurons and amacrine cells that normally regulates photoreceptor function (34).

However, the 2F1 (Fig. 2Bi) responses are almost completely eliminated in the $ort^{-/-}$ flies (Fig. 2Bii and iii)—as would be expected if they were a result of transient synaptic firing. The 2F1 response in these *ort* mutants is only evident at high contrast, where it is ∼20% of the wild-type, though significantly (one-tail t-test, $P < 0.05$) above the system noise (Fig. 2Biii). This residual response could arise from a number of sources. Most likely, it derives from the small on- and off-transients in the polarization/depolarization cycle inherent to the photoreceptors themselves [as shown in intracellular photoreceptor recordings, e.g. (35)]. It is also possible that transmission can occur through other, indirect routes (e.g. other types of histamine receptors or gap junctions). A last possibility that this *ort* mutation does not block photoreceptor output completely seems unlikely based on previous recordings (33). The data from Figure 2 indicate that a significant fraction of the second harmonic response originates from neuronal signalling mechanisms and synaptic transmission rather than from the photoreceptors.

Finally, the fourth-order intermodulation term 2F1+2F2 is entirely abolished, with the level of the signal similar to the system noise (Fig. 2C). This suggests that the 2F1+2F2 signalling is entirely neuronal.

Thus, the 2F1 and 2F1+2F2 components depend on synaptic transmitter release by the photoreceptors and so these components indicate signalling downstream of the sensory neurons. This is encouraging because it allows us to make direct comparisons between neuronal data in flies and vertebrates (particularly humans).

Contrast response functions in Drosophila

We designed our experiments to deliver stimuli similar to those used in earlier human and animal work. These stimuli sweep through different contrast levels, allowing us to measure and analyse population-level contrast versus response functions (CRFs). The measurement of these CRFs is important. Sensory neurons must adjust their sensitivity in order to ensure that they signal changes in the environment efficiently. To achieve this, they scale their sensitivity by a factor related to the average amplitude of the local spatiotemporal input. This 'normalization' appears to be a canonical computation that is also found across different parts of the central nervous system and in a wide variety of different organisms (36). When this multiplicative scaling is applied to the input stage, it results in a stereotypical rightward shift of the logarithmic input versus output function of the neuron that has been observed in a wide variety of experiments (25,27,37–41). In addition, some systems also demonstrate 'response gain': a scaling of the outputs rather
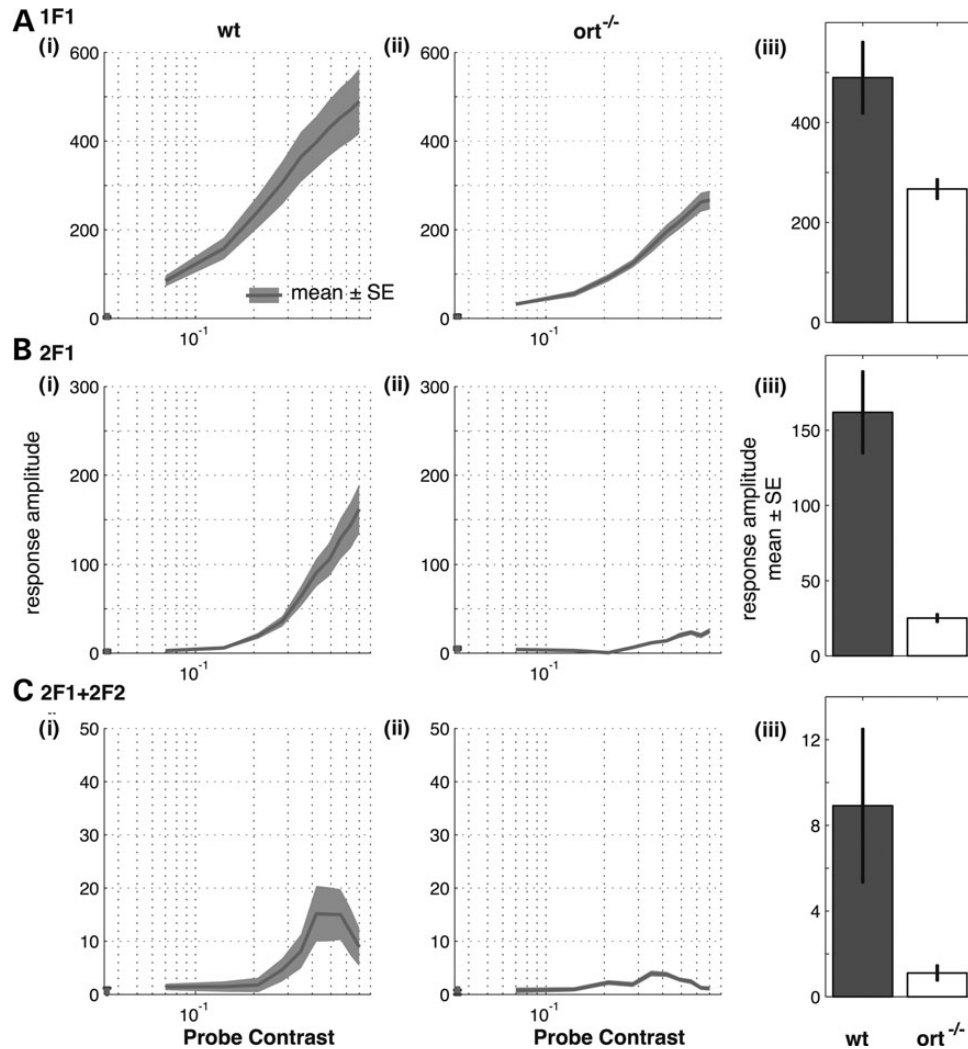
Figure 2. Separation of photoreceptor from neuronal signalling. Harmonic and intermodulation plots from control flies (wt, left column) and ort mutant flies (ort$^{-/-}$, right column). This ort mutation inactivates the histamine A receptor leading to an absence of photoreceptor → second-order neuron synaptic transmission. Flies carrying this mutation exhibit moderately reduced first harmonic (F1) responses (**A**) but their second harmonic (2F1, **B**) and intermodulation terms (2F2+2F1, **C**) are effectively abolished. We interpret this as evidence that the first harmonic is due primarily to on/off responses from the photoreceptors while the 2F1 and 2F2+2F1 terms are generated by neuronal signalling. $N = 17$ (wt), 16 (ort); all flies have white eyes and were 1 day old. The solid line indicates the mean response, with the shaded area as ± 1 standard error.

than the inputs, resulting in a downward compression of the response versus contrast curve. It has been observed that both types of gain control can result from a single type of multiplicative input modulation with differences between contrast and response gain control arising from differences in the size and specificity of the gain pool (42).

In the *Drosophila* experiments described here, we therefore swept the temporal contrast of the 'probe' stimuli through a range of values (0–69%) and measured responses to these stimuli both in isolation, and in the presence of a 30% contrast mask at a different temporal frequency. Performing the experiments using 'frequency tagging' in this manner allows us to measure the effects of stimulus and mask contrast in isolation even though they are superimposed in the stimulus. If the *Drosophila* nervous system exhibits the type of gain control found in other organisms, we expect to see a reduction in the probe

response when the constant mask contrast is presented at the same time.

Response versus contrast

Robust CRFs from control flies (white eyed, +, day 1) are shown in Figure 3. Unmasked responses (shown in grey) from both the first (1F1) and second (2F1) harmonic components of the swept probe (Fig. 3Ai and ii, respectively) increase monotonically with contrast and we can measure reliable signal amplitudes over the entire non-zero contrast range. This high signal-to-noise ratio is a feature of SSVEP recordings and derives from the fact that hundreds of instances of each stimulus condition are averaged together in a phase-sensitive manner and out-of-band noise can be rejected entirely. Fitting a three-parameter hyperbolic ratio function, as in human studies (25,43), provides a smooth
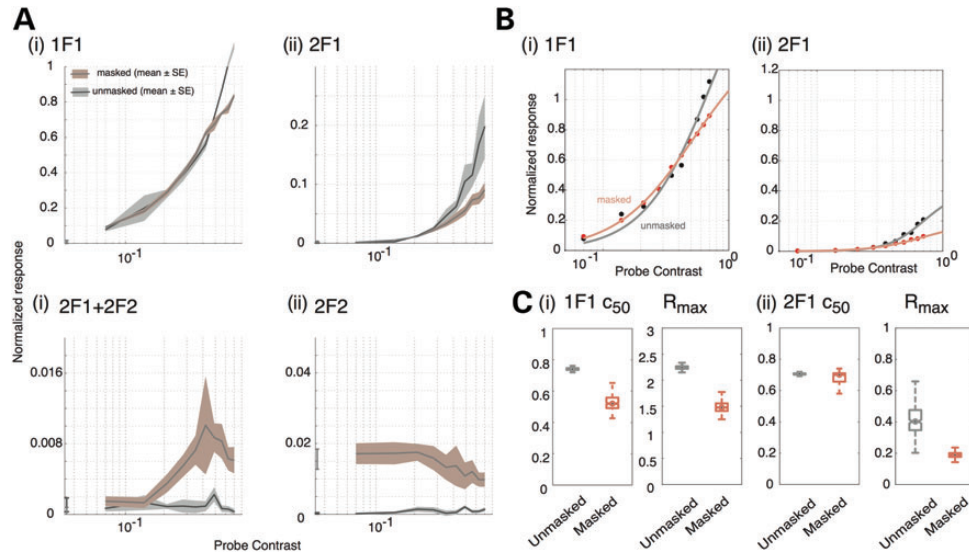
Figure 3. Neural responses to swept contrast flicker in wild-type (*wt*) Drosophila closely resemble those from human data. (**A**) Contrast response functions for (i) 1F1, (ii) 2F1, (iii) 2F1+2F2 with (red) and without (grey) a 30% mask as the probe contrast is increased from 0 to 70%; while (iv) shows the amplitude of the 2F2 response to 30% mask, as the probe contrast is increased. (**B**) Plots of the fitted hyperbolic ratio function $\{R_{max}[c^n/(c^n + c_{50}^n)]\}$ for data in corresponding panels in (A). (**C**) The estimated c_{50} and R_{max} for masked and unmasked data for the data shown in (Ai) and (Aii). Masking has little effect on the 1F1 response, but ~halves R_{max} for the 2F1 response. In (A), the solid line indicates the mean response, with the shaded area as ± 1 standard error. Data from 6 one-day-old white-eyed flies.

curve that passes through the mean data for both the 1F1 and 2F1 data points (Fig. 3B).

Masking and intermodulation

When a mask contrast is applied at a different frequency (F2), the response to the swept input probe changes. The grey curves show the responses when the mask is absent and are therefore a baseline; the red curves show the response measured in the presence of a constant contrast (30%) mask as the probe contrast increases from 0 to 69% (Fig. 3). Responses at 1F1, 2F1, 2F2+2F1 and 2F2 are shown in Figure 3Ai–iv, respectively, and the fitted hyperbolic ratio curves for 1F1 and 2F1 are shown in Figure 3B. The parameters of the hyperbolic fits (Fig. 3C) show that the nature of these changes is different at the 1F1 and 2F1 component frequencies: in the 1F1 response (Fig. 3Bi), our fitting procedures indicate a reduction in the both c_{50} (the semisaturation constant) and R_{max} (the maximum response). In comparison, the change in the 2F1 component is best modelled as a large change in R_{max} with no significant change in c_{50} (Fig. 3Cii). Masking at the neuronal stage therefore manifests as almost a pure response gain change in this phenotype.

The frequency spectrum obtained from a two-input experiment also contains significant power at sums and differences of the input frequencies. In our data (Fig. 3Aiii), these 'intermodulation' responses are maximal around the point at which the mask and probe contrast are equal (30% contrast)—a phenomenon also seen and modelled in our human data (30). When the second input frequency is not present, the response at this intermodulation term is, naturally, flat and gives an estimate of baseline noise levels.

Finally, it is instructive to examine the response at the second harmonic of the mask frequency 2F2 as the probe contrast increases (Fig. 3Aiv). In all our experiments, we see the mask response remaining relatively constant until the probe contrast

matches it. The mask response then declines relatively steeply as the probe contrast increases further. Again, this 'winner-take-all' normalization is a feature of both human EEG and vertebrate single unit experiments (25,30).

Aberrant responses in the *TH>G2019S* model of PD at day 1

We have shown that the SSVEP technique generates CRFs that strongly resemble those of humans, that the 1F1 component represents photoreceptor signalling and that the 2F1 and 2F1+2F2 represent separate stages of the neuronal response. Our hypothesis is that the degeneration seen in old flies expressing *LRRK2-G2019S* was due to hyperactivity at an early age. Therefore, we next ask if the SSVEP technique is powerful enough to reveal small changes due to dopaminergic expression of the PD-related mutation *G2019S* in the youngest flies, when they are 1 day old. We used the *tyrosine hydoxylase* (*TH*) GAL4 (44) to drive expression of either normal human *hLRRK2* or *hLRRK2-G2019S* and compared these with a cross between the GAL4 and wild-type flies (*TH/+*) that do not express a human transgene. Data are displayed in three figures: the raw data in Figure 4, the fitted curves in Figure 5 and the phase data in Figure 6. Statistical analysis is given in Figure 8 and Table 1.

We find that neuronal responses in 1-day-old *TH>hLRRK2* flies are largely similar to those in the *TH/+* controls (Fig. 4). However, we observe significant changes in the visual responses of the *TH>G2019S* flies at this very early stage.

Most strikingly, the contrast sensitivity of the *TH>G2019S* flies is increased dramatically. This results in a shift of the unmasked CRFs relative to the *TH>hLRRK2* and *TH/+*. Because of this shift, the peak neuronal response (2F1 and 2F2) is larger than that seen in controls. The shift in the input/output curve induced by masking is also much larger (Fig. 4B). *TH>G2019S* flies also show a much larger fourth-order intermodulation term (2F1+2F2, Fig. 4D), though the peak of the
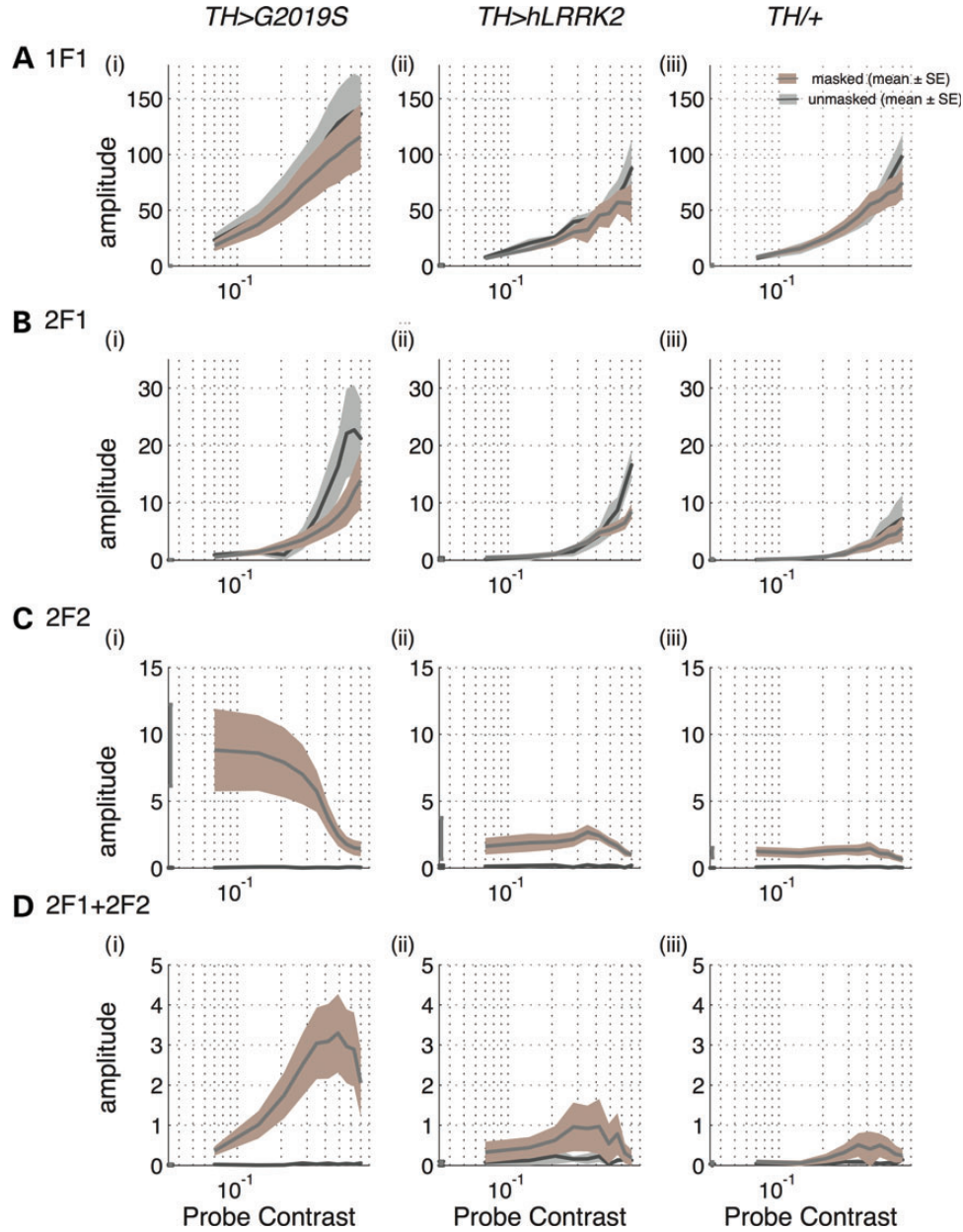
Figure 4. Abnormal visual signalling in 1-day-old flies expressing *LRRK2-G2019S* in their dopaminergic neurons (*TH>G2019S*, left hand column) compared with those expressing wild-type human *LRRK2* (*TH>hLRRK2*, middle column) or outcross controls (*TH/+*, right hand column). Contrast response functions in the *TH>G2019S* flies are substantially steeper (**A**: 1F1 and **B**: 2F1), while the effect of the 30% mask is much stronger (**C**, 2F2). The intermodulation term (2F1+2F2) is also substantially enhanced (**D**). Flies expressing the normal form of *hLRRK2* in the dopaminergic neurons (*TH>hLRRK2*) show visual signalling very close to the control (*TH/+*) flies. Parameter fits for this data are shown in Figure 5, and statistical tests are provided in Table 1. The contrast response function in the presence of the second, masking, input is indicated by the pink shading. The solid lines indicate the mean response; the shaded area ± 1 standard error. $N = 9, 10, 11$.

response still occurs when the contrast of the F2 stimulus component is ∼30% of F1 contrast.

The increased sensitivity of *TH>G2019S* flies could result from a change in either the R_{max} or c_{50} parameter. Estimates of these parameters will also provide the basis for statistical comparison of genotypes and, later in the article, of drugs. We therefore performed bootstrapped fits of the hyperbolic ratio function to the *TH>G2019S*, *TH>hLRRK2* and *TH/+* data. These fits show that the dopaminergic expression of the

PD-associated G2019S genetic variant affects both c_{50} and R_{max} for 1F1 and 2F1 (Fig. 5). The masked R_{max} value for *TH>G2019S* is larger than for the controls (*TH>hLRRK2* and *TH/+*) ($P < 0.01$), but the unmasked values of R_{max} are similar in all three genotypes. This suggests that the masked, but not the unmasked R_{max} parameter at 2F1 distinguishes between the phenotypes—most likely because many of the unmasked curves simply fail to saturate at the contrast levels that we are using, making estimates of maximum response level unreliable.
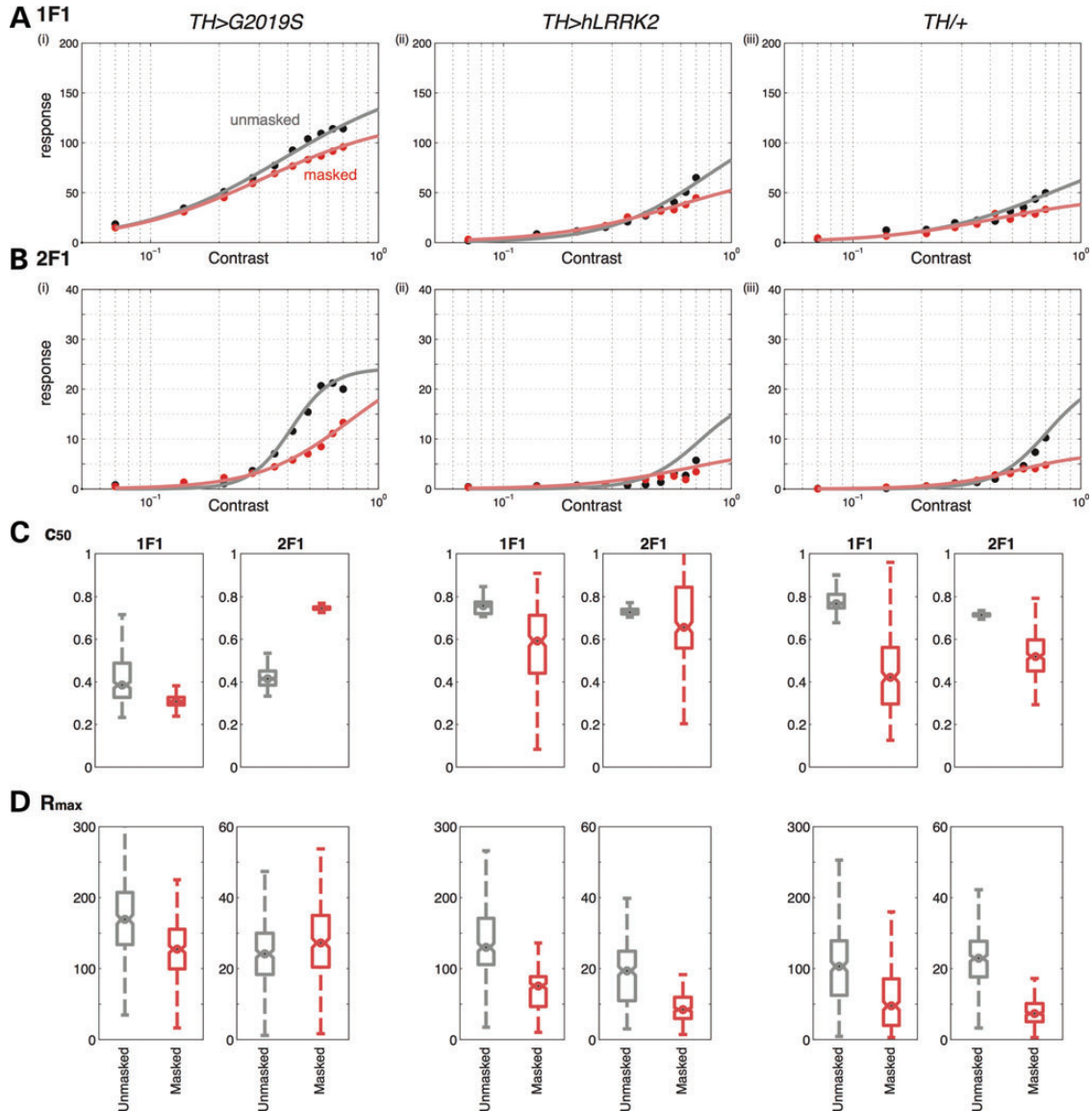
Figure 5. Modelling of the contrast response functions confirms the abnormality of the visual response in 1-day-old *TH>G2019S* flies. Fitting the hyperbolic ratio function for *TH>G2019S*, *TH>hLRRK2* and *TH/+* for 1F1 (**A**) and 2F1 (**B**) provides estimates of c_{50} (**C**) and R_{max} (**D**). These show that expression of *LRRK2-G2019S* in the dopaminergic neurons shifts the 1F1 contrast response function to the left with both the masked and unmasked stimulation. However, the unmasked 2F1 contrast response function shows a leftward shift but masking affects R_{max}. Original data plotted in Figure 4, while statistical tests are provided in Figure 8 and Table 1.

The 1F1 c_{50} of both the unmasked and masked components is reduced to ~50% in *TH>G2019S*, compared with the control flies. The variance is also smaller suggesting consistent differences between the *TH>G2019S* and control flies. Similarly, the unmasked 2F1 c_{50} in *TH>G2019S* is reliably smaller than in the *TH>hLRRK2* and *TH/+* controls. As the 2F1 component originates from the second-order retinal neurons, we have used this parameter in our statistical tests, and find the difference between the unmasked *TH>G2019S* and *TH/+* is highly significant at $P < 0.01$.

A second useful index of neuronal activity is the temporal phase of the SSVEP response (Fig. 6). A common feature of CRFs measured in both humans and animals is that response phase advances with increasing stimulus contrast. This phase advance is predicted by simple biophysical models of gain control that treat sensory neurons as leaky integrators with a contrast-dependent membrane impedance (28,45) Although the phase of an SSVEP signal is related to temporal lags in the signal transduction pathway, its interpretation is complicated by the circular nature of the signal (phase advances and phase lags cannot be disambiguated) and also by the fact that changes in the shape of a complex evoked waveform can generate different phase lags in its constituent frequency components.

It is clear that significant phase shifts between the *TH>G2019S* and *TH/+* responses are present at certain frequencies. In Figure 6, we plot the phases and amplitudes of three representative frequency components (1F1, 2F1 and 2F2) near their maximum amplitudes. For consistency, only data from the masked
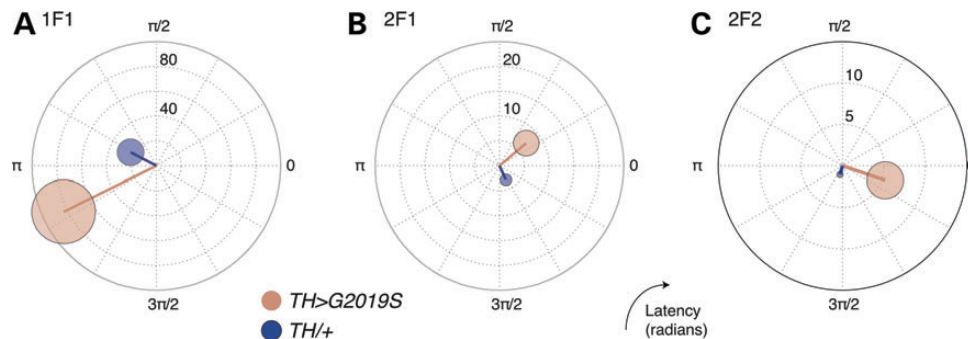
Figure 6. The G2019S mutation changes the response phase of the SSVEP recording. The response lag of the SSVEP signal is shown in polar space with one full cycle of the response corresponding to 2π radians (360 degrees). Lag increases clockwise. (**A**) *TH>G2019S* increases the amplitude of the second harmonic of the first input (2F1) but has little effect on its phase. In comparison, the responses at 2F2 (**B**) and the intermodulation term 2F1+2F2 (**C**) are both larger and phase-shifted with the dopaminergic expression of the *G2019S* mutation. Data from same 1-day-old flies as Figure 4. The one-way MANOVA on the complex data shows that all differences are significant at $P < 0.05$ except for the 2F2 condition, Table 1. An analysis of the complex phase shows that all phase differences are significant at $P < 0.05$.

conditions (which contain both F1 and F2 components) are plotted. Responses at 1F1 differ by just $<1/6$ of a full stimulus period (equivalent to $1/6 * 1/F1$ of a second or approximately 13 ms) with the *TH>G2019S* responses leading those from the *TH/+* controls (Fig. 6A). Responses at 2F1 differ by a little more than a quarter of a cycle, yielding a phase lag for the control animals of ∼12 ms (Fig. 6B). Similarly, we observe a phase shift of slightly more than 1/4 of a cycle in the 2F2 responses. Because a single cycle of the 2F2 frequency (30 Hz) is 1/30 s, this phase shift corresponds to a temporal difference of ∼10 ms, but this estimate is less reliable because of the high variance of the *G2019S* data at this frequency and the relatively small magnitude of the control 2F2 response. These data suggest that the reduced response latency of visual signals in the *TH>G2019S* flies originates in the photoreceptors and is inherited by the second-order laminar neurons.

In summary, we find that expression of *LRRK2-G2019S* in dopaminergic neurons has an effect on both the photoreceptor response (F1), and the neuronal signalling of both the second-order lamina neurons (2F1) and of the neurons which generate the 2F1+2F2 signal (which we suggest is the lamina/medulla system). Modelling suggests that the predominant effect is an increase in both maximum masked response amplitude (R_{max}) and unmasked response sensitivity (c_{50}) in the *TH>LRRK2-G2019S* animals associated with a small reduction in response latency. In old flies, SSVEP analysis shows a reduction in visual gain in the *TH>G2019S* flies, as exemplified by the reduced 2F1 R_{max} (Supplementary Material, Fig. S4). These both confirm our previous data collected using traditional flash electroretinograms (9), and show that SSVEP detects both increased and decreased gain in the *TH>G2019S* flies at young and old ages respectively.

The changes in visual response sensitivity that we observe in flies carrying the *TH>G2019S* mutation appear to be a biomarker for this mutation. Biomarkers such as these are interesting because they allow us to assay the effect of potential therapeutic compounds targeted at the LRRK2 protein. The *G2019S* mutation lies within the kinase domain of this protein, rendering it constitutively active. We therefore asked whether the biomarker we have identified in flies could be used to test a novel class of candidate PD drugs that are specifically targeted at the human LRRK2 kinase domain.

Kinase inhibitors restore wild-type CRFs

Previous work has identified LRRK2-IN-1 (22) as a useful reference compound for LRRK2 kinase inhibition. We have now synthesized BMPPB-32, a novel LRRK2 inhibitor identified from the patent literature (Fig. 7A). Biochemical and cell-based assays show potent inhibition of kinase activity of both wild-type and G2019S variants of hLRRK2. In a biochemical Lantha-Screen® assay (Fig. 7B), BMPPB-32 inhibited hLRRK2 and G2019S with apparent Ki's of 1.5 and 6 nM, respectively. In HEK293 cells, apparent IC50 values of BMPPB-32 on LRRK2 WT, the overactive variant G2019S and the LRRK2-IN-1 inhibition-resistant mutant A2016T were 34, 94 and 64 nM, respectively (Fig. 7C). Profiling using large kinase panels suggests that BMPPB-32 is a selective LRRK2 inhibitor at physiologically relevant ATP concentrations, with good selectively for LRRK2 (Supplementary Material, Figs S1–S3, Results, Table S1). We therefore applied 2.5μM BMPPB-32 throughout larval life, finding that 1-day-old flies contained 37 ng BMPPB-32 pr. g fly tissue. (Supplementary Material, Results). We then measured the effects on the SSVEP responses on 1-day-old adult flies which had been treated either with BMPPB-32 or LRRK2-IN-1.

Figure 8A shows the effects of these two kinase inhibitors on the 2F1 components of the frequency-tagged responses in *TH>G2019S* flies, in comparison with the wild-type (*TH/+*) and untreated *TH>G2019S*. Whereas, as noted above, the *TH>G2019S* has a much steeper CRF, with greater masking, both kinase inhibitors restored the *TH>G2019S* CRF to a shape similar to that of the control flies. Masking also appears similar to control levels. Both LRRK2-IN-1 and BMPPB-32 affect the complete *TH>G2019S* phenotype (Fig. 8B, statistics in Table 1), rescuing the photoreceptor (1F1) and neural response (2F1+2F2). We also examined the effect of the kinase inhibitors on the phase of the 1F1 responses, and found that both drugs reverted the phase change of the *TH>G2019S* flies (Fig. 8C).

We noted previously that the most salient effect of the *LRRK2-G2019S* mutation was to increase the sensitivity of the unmasked 1F1 and 2F1 responses and reduce the maximum amplitude of the masked response. The sensitivity change corresponds to a reduction in the semisaturation constant (c_{50}) when the curves
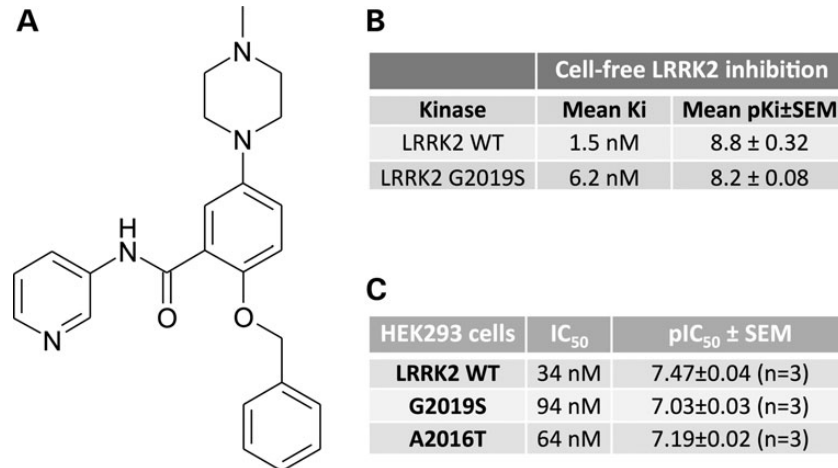
Figure 7. BMPPB-32 structure and LRRK2 kinase inhibition. (**A**) Chemical structure of BMPPB-32. (**B**) Biochemical Ki values obtained in the Lanthascreen LRRK2 activity assay using the mammalian cell purified LRRK2 WT and G2019S protein from Life Technologies. (**C**) Cell-based LRRK2-pSer935 IC50 values obtained in HEK293 cells transiently transfected with either wild-type LRRK2, the PD-relevant G2019S or the inhibition-resistant mutant A2016T.

Table 1. Statistical analysis of the effects of LRRK2-IN-1 and BMPPB-32 on the *TH>G2019S* responses shown in Figure 8

Fig	Parameter	*TH>G2019S versus TH/+* (no drugs)	*TH>G2019S* LRRK2-IN-1 versus no drug	BMPPB-32 versus no drug
8B	1F1	**	NS	NS
	2F1	*	*	NS
	2F2	NS	NS	NS
	2F1+2F2	**	**	NS
8C	1F1 phase	**	*	*
8D	2F1 c_{50}	***	***	$P = 0.06$
	2F1 R_{max}	***	***	**

$*P < 0.05$, $**P < 0.01$, $***P < 0.001$.

are fitted with a hyperbolic ratio function, while the amplitude change corresponds to an increase in the R_{max} parameter. In Figure 8D, we plot these parameters (c_{50} for the unmasked 2F1 component, R_{max} for the masked 2F1) for the four phenotypes listed above. The reduction in c_{50} in the *TH>G2019S* animals is highly significant, while no significant difference is observed between the control (*TH/+*) and LRRK1-IN-1 drug-treated animals, indicating that this kinase inhibitor is effective in restoring wild-type neuronal sensitivity. Similar effects are measured for the R_{max} parameter. The BMPPB-32 kinase inhibitor has qualitatively similar effects to LRRK2-IN-1 with a statistically significant restoration of R_{max} and a near-significant increase in c_{50}. BMPPB-32 also reverts the loss of visual neuronal gain seen in 14-day-old *TH>G2019S* flies (Supplementary Material, Fig. S4).

Off-target effects

One problem in any drug assay is off-target effects. For example, an inhibitor targeted at the kinase domain of one protein may bind to other proteins that have similar kinase domain structure thereby rendering its use as a therapeutic agent problematic. To examine the potential off-target effects of the two compounds tested above, we measured SSVEPs in *dLRRK⁻* flies, in which the homologous *dLRRK* gene has been knocked out. CRFs in these flies resemble those of the *TH/+* controls (compare Fig. 9Ai and ii). The probe (2F1) and mask (2F2) responses in the *dLRRK⁻* flies resemble those of the outcross controls, although the variance is slightly greater. When LRRK2-IN-1 is applied, a severe change in phenotype is seen, with an increase in amplitude of both signals (Fig. 9A and Biii) and strong masking shift (Fig. 9Biii). This may indicate that LRRK2-IN-1 is binding to other kinases, perhaps those related to (mammalian) MAPK7 or DCLK2 (22)—see also Supplementary Material, Figures S1–S3 and Results. However with BMPPB-32, there is no significant change in the CRFs in the *dLRRK⁻* knockout (Fig. 9A and Biv), suggesting this compound has no major off-target effects affecting the SSVEP. This is consistent with the clean kinase selectivity profile of BMPPB-32 in mammalian cells (Supplementary Material, Figs S1–S3 and Results).

DISCUSSION

We have developed and applied the SSVEP technique to *Drosophila*, measuring contrast-driven responses at multiple visual processing stages. Neuronal responses measured in this manner show an intriguing functional homology with those measured in vertebrates.

Using these SSVEP measurements, we show that the presence of a PD-related human transgene affects visual processing and that such changes are reversible *in vivo* by drug treatment.

Functional homology

In most respects, our SSVEP data from *Drosophila* mimic those observed in other species. Our stimulation paradigms were adapted directly from those used in humans (25,27,30,46) and cats (25,28). As in these papers, we found that responses at the probe frequency increased with contrast and exhibited multiplicative masking in the presence of a second, constant contrast component. The response at the mask frequency exhibited a non-linear 'winner-take-all' behaviour—remaining relatively
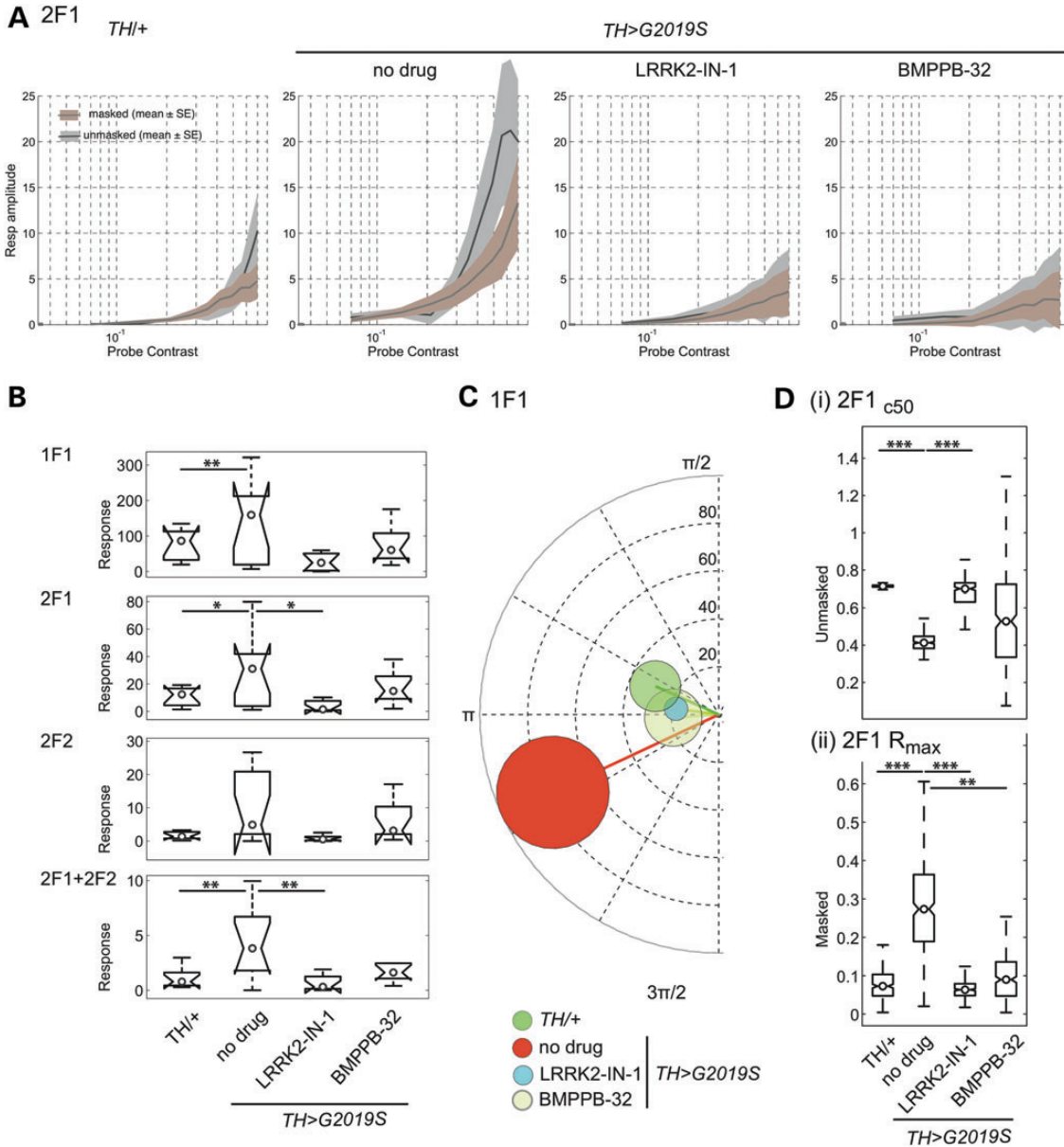
Figure 8. Kinase inhibitors targeted at LRRK2 restore normal responses in the presence of *TH>G2019S* at day 1. Data from four phenotypes are displayed: control (*TH/+*), untreated *TH>G2019S* and *TH>G2019S* flies raised on food containing kinase inhibitor drugs LRRK2-IN-1 or BMPPB-32 at 2.5 μM concentrations. (**A**) Contrast response functions for 2F1 show the increased signalling in *TH>G2019S* is reverted by LRRK2-IN-1 or BMPPB-32. (**B**) Average responses and data spread measured at a single contrast and mask level for different frequency components. The 1F1 signals derive primarily from the photoreceptor responses and are evaluated at 63% probe contrast. 2F1 signals are transient neuronal responses to the same input. 2F2 components derive from neuronal responses to the mask in the presence of a very weak probe input (30% mask contrast, 7% probe contrast). The 2F1+2F2 intermodulation term is likely to arise from non-linear interactions in deeper neuronal structures—here we evaluate it at its peak, which occurs when the probe and mask contrasts are approximately equal (probe = 35% contrast, mask = 30% contrast). At 1F1, 2F1 and 2F1+2F2, the presence of the *hLRRK2-G2019S* transgene elevates the response amplitude significantly ($P < 0.05$, Table 1). Responses from animals raised on 2.5 μM LRRK2-IN-1 are restored and statistically indistinguishable from those of the controls. The compound BMPPB-32 at 2.5 μM concentration also reduced the response amplitude at these frequencies, although the reduction only reached statistical significance in the intermodulation term (2F1+2F2). The responses of G2019S flies are notably more variable across individuals than those of the other organisms. (**C**) Phase plots for unmasked 1F1, showing that both LRRK2-IN-1 and BMPPB-32 restore control-level neuronal SSVEP responses phases measured at 63% probe contrast. Error circles are computed on the complex data using the t-circ statistic. (**D**) Estimated c_{50} values for each of the four phenotypes in (A), showing that the c_{50} value for *TH>G2019S* is approximately half that of the wild-type outcross (*TH/+*). Both kinase inhibitors restore the wild-type value. Statistical tests for the data shown in (B–D) are shown in Table 1. (In B and D, the plots show mean, 95% confidence intervals and data range. $n = 10, 11, 12, 10$.)

constant until the point at which the mask and probe contrasts were equal, then decaying rapidly (25). We also observed robust second (1F1+2F1) and fourth (2F1+2F2) order non-linear intermodulation terms that peaked when the probe and mask were equal in contrast (30). These results suggest that many of the computations involved in luminance and contrast processing are conserved between the early stages of the mammalian and *Drosophila* visual systems.
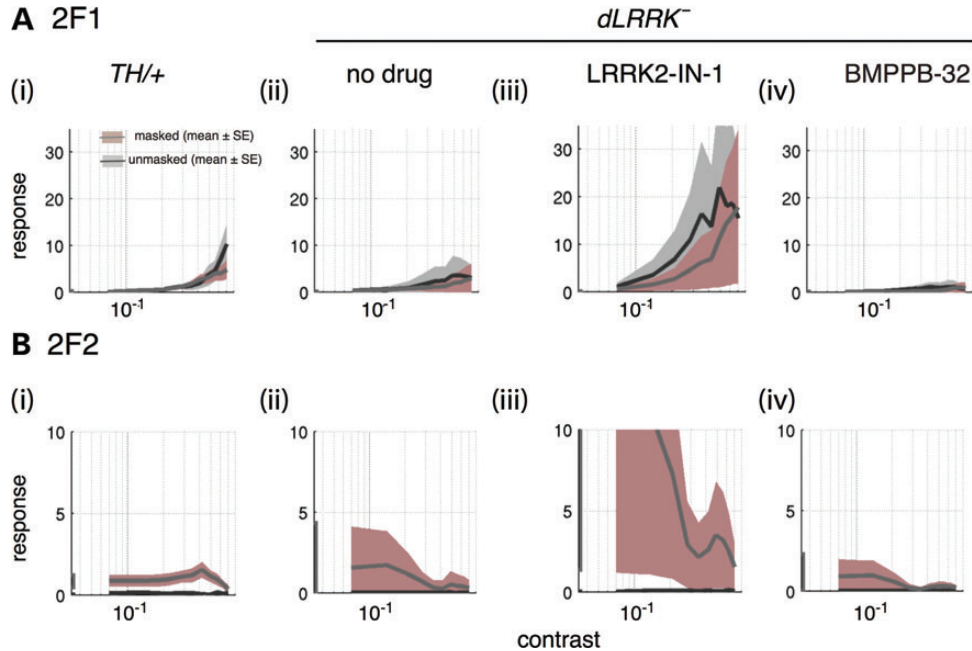
Figure 9. Off-target effects of LRRK2 kinase inhibitors. The contrast response functions (**A**) 2F1 and (**B**) 2F2 of the *dLRRK⁻* knockout are similar to those of wild-type flies (*TH/+*). Application of 2.5 μM LRRK2-IN-1 produces a marked phenotype (increased amplitude, stronger mask), while BMPPB-32 has no effect. This suggests that LRRK2-IN-1 has an off-target effect, as the *dLRRK⁻* knockout has no LRRK2 homolog. $n = 10, 18, 7, 8$.

We also note some differences between our results and those from other organisms. While we observe strong masking of the neuronal responses, this is best described by response gain control (a reduction in the maximum firing rate) rather than the contrast-gain control (a decrease in sensitivity) as observed in other organisms (25,27,30). The reason for this is unclear. One explanation may be that our response curves do not saturate—possibly because we are using a zero-dimensional stimulus that drives spatially tuned neurons only weakly. In addition, our light source was monochromatic and short wavelength which may have slowed the reconversion of metarhodopsin to rhodopsin in the phototransduction cascade, thereby reducing the overall temporal sensitivity of the preparation (47–49). Without a saturating response, it is difficult to distinguish changes in response gain from changes in contrast gain unambiguously and it is possible that both effects are present in our data. Finally, our stimulus drove responses across much of the visual field exciting essentially all neurons in the visual system to some degree. It is possible that masking in *Drosophila* depends on the spatial configuration and extent of stimuli as it does in the human visual system (50,51) and that altering the relative sizes of the excitatory and inhibitory stimulus components can lead to a range of contrast response functions that encompass both response- and contrast-gain effects (42).

Effects of the PD-related LRRK2-G2019S

We find that expressing *LRRK2-G2019S* in the dopaminergic neurons affects neural signalling in the retinal network at day 1, and that this is manifest as an increase in sensitivity, masking, intermodulation and shorter latency. These characteristics suggest that visual neurons may be depolarized, and unable to maintain their resting membrane potential because they cannot synthesize enough ATP to pump cations across the plasma membrane fast enough. Knockout of another PD-related gene, *parkin*, also results in membrane depolarization (52). Although losses of photoreceptor function and disorganization in the regular lattice of ommatidia have been seen when *LRRK2* and other PD-related genes (e.g. α-*synuclein*) were manipulated (9,53,54), the reason for this neurodegeneration was unknown. Hindle *et al.* (9) showed that increasing neuronal activity accelerated the loss of photoreceptor function, which was associated with mitochondrial decay and possible problems with ATP synthesis. Now our data provide support for the idea that extra (unregulated) neuronal activity is an early step towards neuronal degeneration.

In *Drosophila* larvae, the rate of transmitter release at the neuromuscular junction was slowed by *LRRK2-G2019S* expression (16,17). Our data do not allow us to separate changes in neuronal excitability from changes in transmitter release. However, we note that exogenous dopamine slows the speed of the isolated photoreceptor response (10), while visual response negatively correlates with dopamine levels in the brain (55). Thus, if *LRRK2-G2019S* expression in the dopaminergic neurons reduces the release of dopamine, we would expect a faster visual response. This is commensurate with our phase data, which showed a decrease in latency of 10–13 ms at the photoreceptors. A similar change in latency was inherited by the second-order neurons.

However, there is a major difference between the previous neuromuscular junction experiments (16,17); and our work in the ways in which *LRRK2-G2019S* was expressed. Their recordings were made from synapses at which the transgene was expressed both pre- and post-synaptically, but our biggest difference comes from neurons (in the lamina, medulla) in which *LRRK2-G2019S* was not expressed. Rather the lamina and

medulla neurons surround the dopaminergic neurons in which the *G2019S* transgene was expressed. An impact on surrounding neurons of expressing *G2019S* suggests non-autonomous actions, as proposed by Braak *et al*. (56) and reported from human and animal studies of another PD-related gene, α-synuclein (57–59).

In-vivo testing of kinase function of LRRK2

A consistent feature of *LRRK2-G2019S* in biochemical assays is elevated kinase activity compared with wild-type *hLRRK2* (21). Our day 1 visual data also show a marked difference between *TH>hLRRK2* and *TH>G2019S*, which is reduced by kinase inhibitors LRRK2-IN-1 and BMPPB-32, suggesting that the kinase function is crucial in the whole organism as well as in biochemical and cell culture assays. The use of *dLRRK⁻* flies, in which no LRRK homolog is present, discriminates the two inhibitors, BMPPB-32 and LRRK2-IN-1, with the latter providing marked off-target effects.

A wide range of kinase inhibitors are being developed for inhibition of LRRK2 (60,61), but little testing has been done in the whole organism. Two kinase inhibitors, GW5074 and sorafenib, have been tested in *Drosophila* lifespan and climbing assays, and provided some extension of lifespan (62). Their median lifespan was 12–13 weeks, making our fly assay much faster (<14 days treatment, <1 h recording/and analysis per fly).

Our SSVEP assay therefore provides a robust and stable platform, with quantitative outputs that gives insights into basic neuronal processing, mechanisms of gain control, suggesting homology in retinal function between flies and mammals, and can be used for assessing the effectiveness and selectivity of drug development candidates.

MATERIALS AND METHODS

Fly stocks and genetics

Stock vials of *Drosophila melanogaster* were kept on yeast-sucrose-agar fly food (63). The GAL4/UAS system was used for targeted gene expression using the UAS-constructs UAS-*hLRRK2* or UAS-*G2019S* (64), and *TH*-GAL4 (44), to achieve expression in the dopaminergic neurons. For controls, we crossed *TH*-GAL4 with a white-eyed wild-type (w^{1118}, herein +). These fly crosses were used for direct comparison with our previous paper (9). The *dLRRK⁻* line, also known as e03680 (65,66), is a complete knockout of the fly homolog to *LRRK2*. In developing the technique, we also used the histamine receptor A null $ort^{-/-}$ (ort^{US6096}, also known as ort^5) strain (33). As these flies have white eyes, we compared their visual response with w^{1118} flies. Experimental flies were kept in a 12 h light on:12 h off constant temperature room (25°C), and allowed to lay eggs on instant fly food (Carolina Biological Supply). After 2 days, the adult flies were removed. Vials were inspected daily, females collected and the visual response was tested within 10–18 h of eclosion.

Preparation

Female flies were aspirated out of their vial into a shortened pipette tip. Once the head emerged, each fly was secured with a small droplet of nail polish (Creative Nail Design) (Fig. 1A) and the fly was allowed to recover in the dark for ~10 min. The fly was illuminated by a blue light from an LED. The intensity was controlled by a sequence generator encoded in Matlab. In some parts of the sequence, we delivered a single square wave, flickering about the mean illumination at a frequency of 12 Hz. This stimulus we called the 'probe'. In other parts of the sequence, we delivered a wave made up of the sum of two square waves, one at 12 Hz and the other at 15 Hz. In this case we refer to the second, 15 Hz component as the 'mask'. We used square waves to reflect the stimuli used in our earlier drosophila ERG experiments (9) and SSVEP experiments with human subjects (30). We placed a single electrode on the surface of the Drosophila eye and recorded a single waveform in response to each stimulus sequence. Each stimulus sweep gave a signal well above the system noise, so that a phase-locked response is evident (Fig. 1C). These time series were analysed in the frequency domain using a Fourier transform from which the scalar amplitude (Fig. 1D) and phase, or temporal 'lag' (Fig. 1E) of individual frequency components was extracted (67). Full details of the apparatus and recording method are presented in Supplemental Material.

Kinase inhibitors

We tested the effect on fly vision of two potential LRRK2 kinase inhibitors. One, BMPPB-32 is novel and fully characterized in the Supplementary Material. There we report its synthesis, biochemical and cellular properties, role as a kinase inhibitor and uptake to the CNS. The second inhibitor is LRRK2-in-1 (Division of Signal Transduction Therapy (DSTT) Unit at the University of Dundee). Stock solutions in ethanol were kept at −20°C until the day of use. The solution was diluted into de-ionized water, and mixed with the Instant Fly Food compound, making the final concentration 2.5 μм. Adults (8–10 female, 3–5 male flies) were allowed to lay eggs on the food for 2 days and then removed. Larvae were allowed to develop into pupae, and the emerging adults collected between 4 and 18 h.

SUPPLEMENTARY MATERIAL

Supplementary Material is available at *HMG* online.

REFERENCES

1. Archibald, N.K., Clarke, M.P., Mosimann, U.P. and Burn, D.J. (2009) The retina in Parkinson's disease. *Brain*, **132**, 1128–1145.

2. Witkovsky, P. (2004) Dopamine and retinal function. *Doc. Ophthal.*, **108**, 17–39.

3. Jackson, C.R., Ruan, G.-X., Aseem, F., Abey, J., Gamble, K., Stanwood, G., Palmiter, R.D., Iuvone, P.M. and McMahon, D.G. (2012) Retinal dopamine mediates multiple dimensions of light-adapted vision. *J. Neurosci.*, **32**, 9359–9368.

4. Harnois, C. and Di Paolo, T. (1990) Decreased dopamine in the retinas of patients with Parkinson's disease. *Invest. Opthal. Vis. Sci.*, **31**, 2473.

5. Cajal, S.R. and Sanchez, D. (1915) Contribucion al conocimiento de los centros nerviosos de los insectos. Parte 1. Retina y centros opticos. *Trab. Lab Invest. Biol. Univ. Madrid*, **13**, 1–168.

6. Sanes, J.R. and Zipursky, S.L. (2010) Design principles of insect and vertebrate visual systems. *Neuron*, **66**, 15–36.

7. Nassel, D.R. and Elekes, K. (1992) Aminergic neurons in the brain of blowflies and Drosophila: dopamine- and tyrosine hydroxylase-immunoreactive neurons and their relationship with putative histaminergic neurons. *Cell Tissue Res.*, **267**, 147–167.

8. Nassel, D.R., Elekes, K., Johansson, K.U. and Nässel, D.R. (1988) Dopamine-immunoreactive neurons in the blowfly visual system: light and electron microscopic immunocytochemistry. *J. Chem. Neuroanat.*, **1**, 311–325.

9. Hindle, S.J., Afsari, F., Stark, M., Middleton, C.A., Evans, G.J.O., Sweeney, S.T. and Elliott, C.J.H. (2013) Dopaminergic expression of the Parkinsonian gene LRRK2-G2019S leads to non-autonomous visual neurodegeneration, accelerated by increased neural demands for energy. *Hum. Mol. Genet.*, **22**, 2129–2140.

10. Chyb, S., Hevers, W., Forte, M., Wolfgang, W.J., Selinger, Z. and Hardie, R.C. (1999) Modulation of the light response by cAMP in Drosophila photoreceptors. *J. Neurosci.*, **19**, 8799–8807.

11. Healy, D.G., Falchi, M., O'Sullivan, S.S., Bonifati, V., Durr, A., Bressman, S., Brice, A., Aasly, J., Zabetian, C.P., Goldwurm, S. *et al.* (2008) Phenotype, genotype, and worldwide genetic penetrance of LRRK2-associated Parkinson's disease: a case-control study. *Lancet Neurol.*, **7**, 583–590.

12. Paisán-Ruiz, C., Lewis, P.A. and Singleton, A.B. (2013) LRRK2: cause, risk, and mechanism. *J. Parkinsons. Dis.*, **3**, 85–103.

13. Beal, M. (2010) Parkinson's disease: a model dilemma. *Nature*, **466**, S8–S10.

14. Tong, Y., Yamaguchi, H., Giaime, E., Boyle, S., Kopan, R., Kelleher, R.J. and Shen, J. (2010) Loss of leucine-rich repeat kinase 2 causes impairment of protein degradation pathways, accumulation of alpha-synuclein, and apoptotic cell death in aged mice. *Proc. Natl Acad. Sci. USA*, **107**, 9879–9884.

15. Ng, C.-H., Guan, M.S.H., Koh, C., Ouyang, X., Yu, F., Tan, E.-K., O'Neill, S.P., Zhang, X., Chung, J. and Lim, K.-L. (2012) AMP kinase activation mitigates dopaminergic dysfunction and mitochondrial abnormalities in drosophila models of Parkinson's disease. *J. Neurosci.*, **32**, 14311–14317.

16. Matta, S., Van Kolen, K., da Cunha, R., van den Bogaart, G., Mandemakers, W., Miskiewicz, K., De Bock, P.-J., Morais, V.A., Vilain, S., Haddad, D. *et al.* (2012) LRRK2 controls an EndoA phosphorylation cycle in synaptic endocytosis. *Neuron*, **75**, 1008–1021.

17. Lee, S., Liu, H.-P., Lin, W.-Y., Guo, H. and Lu, B. (2010) LRRK2 kinase regulates synaptic morphology through distinct substrates at the presynaptic and postsynaptic compartments of the Drosophila neuromuscular junction. *J. Neurosci.*, **30**, 16959–16969.

18. Paulk, A.C., Zhou, Y., Stratton, P., Liu, L. and van Swinderen, B. (2013) Multichannel brain recordings in behaving Drosophila reveal oscillatory activity and local coherence in response to sensory stimulation and circuit activation. *J. Neurophysiol.*, **110**, 1703–1721.

19. Van Swinderen, B. (2012) Competing visual flicker reveals attention-like rivalry in the fly brain. *Front. Integr. Neurosci.*, **6**, 96.

20. Laughlin, S. (1981) A simple coding procedure enhances a neuron's information capacity. *Z. Naturforsch. C.*, **36c**, 910–912.

21. Greggio, E. and Cookson, M.R. (2009) Leucine-rich repeat kinase 2 mutations and Parkinson's disease: three questions. *ASN Neuro*, **1**, e00002.

22. Deng, X., Dzamko, N., Prescott, A., Davies, P., Liu, Q., Yang, Q., Lee, J.-D., Patricelli, M.P., Nomanbhoy, T.K., Alessi, D.R. *et al.* (2011) Characterization of a selective inhibitor of the Parkinson's disease kinase LRRK2. *Nat. Chem. Biol.*, **7**, 203–205.

23. Fischbach, K.-F. and Dittrich, A.P.M. (1989) The optic lobe of Drosophila melanogaster. I. A Golgi analysis of wild-type structure. *Cell Tissue Res.*, **258**, 441–475.

24. Porciatti, V., Pizzorusso, T. and Maffei, L. (1999) The visual physiology of the wild type mouse determined with pattern VEPs. *Vision Res.*, **39**, 3071–3081.

25. Busse, L., Wade, A.R. and Carandini, M. (2009) Representation of concurrent stimuli by population activity in visual cortex. *Neuron*, **64**, 931–942.

26. Burr, D.C. and Morrone, M.C. (1987) Inhibitory interactions in the human vision system revealed in pattern-evoked potentials. *J. Physiol.*, **389**, 1–21.

27. Candy, T.R., Skoczenski, A.M. and Norcia, A.M. (2001) Normalization models applied to orientation masking in the human infant. *J. Neurosci.*, **21**, 4530–4541.

28. Carandini, M. and Ferster, D. (1997) A tonic hyperpolarization underlying contrast adaptation in cat visual cortex. *Science*, **276**, 949–952.

29. Heisenberg, M. (1971) Separation of receptor and lamina potentials in the electroretinogram of normal and mutant Drosophila. *J. Exp. Biol.*, **55**, 85–100.

30. Tsai, J.J., Wade, A.R. and Norcia, A.M. (2012) Dynamics of normalization underlying masking in human visual cortex. *J. Neurosci.*, **32**, 2783–2789.

31. Burton, G.J. (1973) Evidence for non-linear response processes in the human visual system from measurements on the thresholds of spatial beat frequencies. *Vision Res.*, **13**, 1211–1225.

32. Regan, D. and Regan, M.P. (1987) Nonlinearity in human visual responses to two-dimensional patterns, and a limitation of Fourier methods. *Vis. Res*, **27**, 2181–2183.

33. Pantazis, A., Segaran, A., Liu, C.-H., Nikolaev, A., Rister, J., Thum, A.S., Roeder, T., Semenov, E., Juusola, M. and Hardie, R.C. (2008) Distinct roles for two histamine receptors (hclA and hclB) at the Drosophila photoreceptor synapse. *J. Neurosci.*, **28**, 7250–7259.

34. Zheng, L., de Polavieja, G.G., Wolfram, V., Asyali, M.H., Hardie, R.C. and Juusola, M. (2006) Feedback network controls photoreceptor output at the layer of first visual synapses in Drosophila. *J. Gen. Physiol.*, **127**, 495–510.

35. Niven, J.E., Vähäsöyrinki, M., Kauranen, M., Hardie, R.C., Juusola, M. and Weckström, M. (2003) The contribution of Shaker K+ channels to the information capacity of Drosophila photoreceptors. *Nature*, **421**, 630–634.

36. Carandini, M. and Heeger, D.J. (2012) Normalization as a canonical neural computation. *Nat. Rev. Neurosci.*, **13**, 51–62.

37. Olsen, S.R., Bhandawat, V. and Wilson, R.I. (2010) Divisive normalization in olfactory population codes. *Neuron*, **66**, 287–299.

38. Schneeweis, D.M. and Schnapf, J.L. (1999) The photovoltage of macaque cone photoreceptors: adaptation, noise, and kinetics. *J. Neurosci.*, **19**, 1203–1216.

39. Louie, K., Grattan, L.E. and Glimcher, P.W. (2011) Reward value-based gain control: divisive normalization in parietal cortex. *J. Neurosci.*, **31**, 10627–10639.

40. Asadollahi, A., Mysore, S.P. and Knudsen, E.I. (2010) Stimulus-driven competition in a cholinergic midbrain nucleus. *Nat. Neurosci.*, **13**, 889–895.

41. Phillips, D.P. (1990) Neural representation of sound amplitude in the auditory cortex: effects of noise masking. *Behav. Brain Res.*, **37**, 197–214.

42. Reynolds, J.H. and Heeger, D.J. (2009) The normalization model of attention. *Neuron*, **61**, 168–185.

43. Lauritzen, T.Z., Ales, J.M. and Wade, A.R. (2010) The effects of visuospatial attention measured across visual cortex using source-imaged, steady-state EEG. *J. Vis.*, **10**, 1–39.

44. Friggi-Grelin, F., Coulom, H., Meller, M., Gomez, D., Hirsh, J. and Birman, S. (2003) Targeted gene expression in Drosophila dopaminergic cells using regulatory sequences from tyrosine hydroxylase. *J. Neurobiol.*, **54**, 618–627.

45. Sit, Y.F., Chen, Y., Geisler, W.S., Miikkulainen, R. and Seidemann, E. (2009) Complex dynamics of V1 population responses explained by a simple gain-control model. *Neuron*, **64**, 943–956.

46. Tsai, J.J., Norcia, A.M., Ales, J.M. and Wade, A.R. (2011) Contrast gain control abnormalities in idiopathic generalized epilepsy. *Ann. Neurol.*, **70**, 574–582.

47. Hillman, P., Hochstein, S. and Minke, B. (1983) Transduction in invertebrate photoreceptors: role of pigment bistability. *Physiol. Rev.*, **63**, 668–772.

48. Kiselev, A. and Subramaniam, S. (1994) Activation and regeneration of rhodopsin in the insect visual cycle. *Science*, **266**, 1369–1373.

49. Xiong, B. and Bellen, H. (2013) Rhodopsin homeostasis and retinal degeneration: lessons from the fly. *Trends Neurosci.*, **36**, 652–660.

50. Solomon, S.G., Lee, B.B. and Sun, H. (2006) Suppressive surrounds and contrast gain in magnocellular-pathway retinal ganglion cells of macaque. *J. Neurosci.*, **26**, 8715–8726.

51. Cavanaugh, J.R., Bair, W. and Movshon, J.A. (2002) Selectivity and spatial distribution of signals from the receptive field surround in macaque V1 neurons. *J. Neurophysiol.*, **88**, 2547–2556.

52. Vincent, A., Briggs, L., Chatwin, G.F.J., Emery, E., Tomlins, R., Oswald, M., Middleton, C.A., Evans, G.J.O., Sweeney, S.T. and Elliott, C.J.H. (2012) Parkin induced defects in neurophysiology and locomotion are generated by metabolic dysfunction and not oxidative stress. *Hum. Mol. Genet.*, **21**, 1760–1769.

53. Venderova, K., Kabbach, G., bdel-Messih, E., Zhang, Y., Parks, R.J., Imai, Y., Gehrke, S., Ngsee, J., LaVoie, M.J. and Slack, R. (2009) Leucine-rich repeat kinase interacts with Parkin, DJ-1 and PINK-1 in a Drosophila melanogaster model of Parkinson's disease. *Hum. Mol. Genet.*, **18**, 4390–4404.

54. Feany, M.B. and Bender, W.W. (2000) A Drosophila model of Parkinson's disease. *Nature*, **404**, 394–398.

55. Calcagno, B., Eyles, D., van Alphen, B. and van Swinderen, B. (2013) Transient activation of dopaminergic neurons during development modulates visual responsiveness, locomotion and brain activity in a dopamine ontogeny model of schizophrenia. *Transl. Psychiatry*, **3**, e206.

56. Braak, H., Del Tredici, K., Rüb, U., de Vos, R.A.I., Jansen Steur, E.N.H. and Braak, E. (2003) Staging of brain pathology related to sporadic Parkinson's disease. *Neurobiol. Aging*, **24**, 197–211.

57. Desplats, P., Lee, H.-J., Bae, E.-J., Patrick, C., Rockenstein, E., Crews, L., Spencer, B., Masliah, E. and Lee, S.-J. (2009) Inclusion formation and neuronal cell death through neuron-to-neuron transmission of alpha-synuclein. *Proc. Natl Acad. Sci. USA*, **106**, 13010–13015.

58. Braak, H. and Del Tredici, K. (2008) Assessing fetal nerve cell grafts in Parkinson's disease. *Nat. Med.*, **14**, 483–485.

59. Mattila, P.M., Rinne, J.O., Helenius, H., Dickson, D.W. and Röyttä, M. (2000) Alpha-synuclein-immunoreactive cortical Lewy bodies are associated with cognitive impairment in Parkinson's disease. *Acta Neuropathol.*, **100**, 285–290.

60. Lee, B.D., Shin, J.-H., VanKampen, J., Petrucelli, L., West, A.B., Ko, H.S., Lee, Y.-I., Maguire-Zeiss, K.A., Bowers, W.J., Federoff, H.J. *et al.* (2010) Inhibitors of leucine-rich repeat kinase-2 protect against models of Parkinson's disease. *Nat. Med.*, **16**, 998–1000.

61. Lee, B.D., Dawson, V.L. and Dawson, T.M. (2012) Leucine-rich repeat kinase 2 (LRRK2) as a potential therapeutic target in Parkinson's disease. *Trends Pharmacol. Sci.*, **33**, 365–373.

62. Liu, Z., Hamamichi, S., Lee, B.D., Yang, D., Ray, A., Caldwell, G.A., Caldwell, K.A., Dawson, T.M., Smith, W.W. and Dawson, V.L. (2011) Inhibitors of LRRK2 kinase attenuate neurodegeneration and Parkinson-like phenotypes in Caenorhabditis elegans and Drosophila Parkinson's disease models. *Hum. Mol. Genet.*, **20**, 3933–3942.

63. Carpenter, J.M. (1950) A new semisynthetic food medium for Drosophila. *Dros. Inf. Serv.*, **24**, 96–97.

64. Liu, Z., Wang, X., Yu, Y., Li, X., Wang, T., Jiang, H., Ren, Q., Jiao, Y., Sawa, A., Moran, T. *et al.* (2008) A Drosophila model for LRRK2-linked parkinsonism. *Proc. Natl Acad. Sci. USA*, **105**, 2693–2698.

65. Imai, Y., Gehrke, S., Wang, H.-Q.Q., Takahashi, R., Hasegawa, K., Oota, E. and Lu, B. (2008) Phosphorylation of 4E-BP by LRRK2 affects the maintenance of dopaminergic neurons in Drosophila. *EMBO J.*, **27**, 2432–2443.

66. Wang, D., Tang, B., Zhao, G., Pan, Q., Xia, K., Bodmer, R. and Zhang, Z. (2008) Dispensable role of Drosophila ortholog of LRRK2 kinase activity in survival of dopaminergic neurons. *Mol. Neurodegener.*, **3**, 3.

67. Bracewell, R. (1978) The Fourier transform and its applications. 2nd ed. New York: McGraw-Hill.